ELSEVIER

Surface Science 426 (1999) L420–L425

surface science

www.elsevier.nl/locate/susc

Surface Science Letters

Field emission interferometry with the scanning tunneling microscope

A.J. Caamaño [a], Y. Pogorelov [b], O. Custance [a], J. Méndez [a], A.M. Baró [a], J.Y. Veuillen [c], J.M. Gómez-Rodríguez [a], J.J. Sáenz [a,*]

[a] *Departamento de Física de la Materia Condensada and Instituto 'Nicolás Cabrera', Universidad Autónoma de Madrid, E-28049 Madrid, Spain*

[b] *Departamento de Física, Universidade do Porto, Rua do Campo Alegre 687, 4150 Porto, Portugal*

[c] *Laboratoire d'Etudes des Propriétés Electroniques des Solides-CNRS, F-38042 Grenoble Cédex 9, France*

Received 1 February 1999; accepted for publication 19 February 1999

Abstract

A scanning tunneling microscope, operated in the near field emission regime, is used to obtain the phases of very low energy electrons reflected from a sample surface. A simple theoretical model shows that the spectrum of the electron standing waves, formed in the vacuum gap between the tip probe and the sample, is directly related to the complex amplitudes of the reflected electron waves. The surface sensitivity of the interferometric spectra is demonstrated in the analysis of different reconstructions of the Pb/Si(111) system.

Keywords: Electron–solid interactions, scattering, diffraction; Field emission; Field ionization; Lead; Scanning tunneling microscopy; Semi-empirical models and model calculations; Silicon; Surface electronic phenomena (work function, surface potential, surface states, etc.)

It has long been recognized that under the influence of an external electric field, electrons can be temporarily trapped in the vicinity of surfaces. These field emission resonances (FER) can be seen as electron standing waves partially confined between the external electrostatic potential and the rapidly changing surface potential. The electron standing waves manifest themselves as resonant peaks in the energy distribution of ions obtained by field ion microscopy (FIM) [1–7] or as oscillations in the field emission current in semiconductor devices [8–11] and scanning tunneling microscopy (STM) [12–19]. It was suggested that FER provides important information about surface electronic structure and adsorbate properties [4,12,13], subsurface atomic positions [14,15], atomic structure [17,18], surface potential [5,20–24], surface properties of buried interfaces [9–11] and surfaces of amorphous samples [19]. However, despite a large theoretical effort [3,6,8,20–25], the physics behind the observed FER spectra has not been completely understood.

In this letter, we present an analyis of the STM-

* Corresponding author. Fax: +34-91-397-3961.
E-mail address: juanjo.saenz@uam.es (J.J. Sáenz)

PII: S0039-6028(99)00346-5

FER spectra within a simple theoretical framework. We will discuss the overall features apparent in most of the experimental data, in order to establish those features that are general to STM electron interferometry and not sample- or probe-tip-specific. As we will show, the puzzling systematic disruptions repetitively observed in the STM-FER spectra of various crystalline samples [12–18] as well as in amorphous surfaces [19] can be easily understood in terms of a simple model.

The analysis of the resonance spectra should offer the unique capability of accessing not only the intensity but also the phases of the reflected electron waves. The phase of the electron wavefunctions is closely related to the fundamental properties of solid surfaces [26–31]. Appelbaum and McRae [6] proposed the use of a field ion energy distribution to measure this phase shift, but, as far as we know, to date, no such information has been obtained [7]. Here, we demonstrate the feasibility of obtaining the phases of the reflected electrons from STM electron interferometry experiments. We present the first experimental results for the phase $\phi(\epsilon)$ versus energy, ϵ curves obtained from the FER spectra of different reconstructions of the Pb/Si(111) system. Since the actual areas probed by STM are in the nanometer range, this may present an important step towards a quantitative surface analysis at the nanoscale.

In the field emission regime (i.e. for applied voltages higher than the sample work function, $eV \geq W_s$), the electric field strength, F_t, at the probe-tip apex determines the current intensity through the Fowler–Nordheim (F–N) equation [32]. Operating the STM in the constant current mode implies then an approximately constant electric field, F_t, at the emitter surface [33]. In the near field emission regime [33–36] (S of the order of, or smaller, than the tip radius, R), the field close to the sample surface is well described [37,38] by $F_s \approx V/S$. However, due to tip curvature effects, the field on the tip apex, F_t, is given by [37,38] $F_t \approx F_s\ (S+R)/R$. At negative tip polarities, the S–V characteristics should then follow a constant F_t trajectory

$$S(V) \approx \frac{V}{F_t}\left(1-\frac{V}{F_t R}\right)^{-1}. \qquad (1)$$

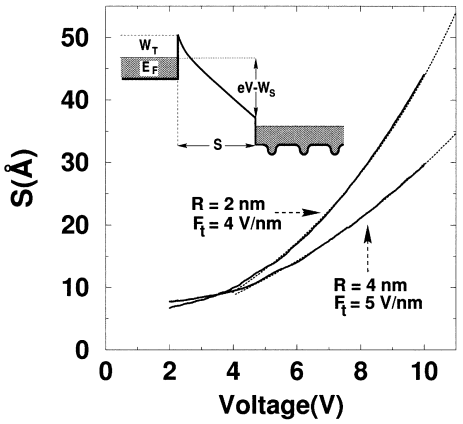

Fig. 1. Inset: Schematic one-dimensional potential energy diagram in the near field emission regime. Main figure: distance–voltage characteristics obtained from a Pb/Si(111)-(R3) spot with two different tips. Dashed lines correspond to the semiclassical theoretical curves for the tip radii and fields indicated in the figure.

On top of this smooth semiclassical curve, the actual S–V curves present small oscillations ΔS. The main physics behind these oscillations can be described in terms of the schematic one-dimensional potential energy curve shown in the inset of Fig. 1. The oscillations were interpreted as being due to the interference of waves reflected from the regions of sharply changing potential at the sample surface [3,8]. Most of the theoretical studies have focused on the influence of the exact shape of the potential [20–24]. However, the matching of the electron wave functions depends not only on the surface potential but also on the structural and electronic properties of the last few atomic layers.

Following an approach similar to that of dynamic low-energy-electron diffraction (LEED) [6,39,40], these properties can be included in the form of a complex amplitude reflection coefficient, r, defined in the absence of any external electric field (Fig. 2). The geometry and the chemical nature of the surface atoms determine the functional dependence of both the modulus $|r(\epsilon)|$ and phase $\phi(\epsilon)$ (with $\epsilon = eV - W_s$; see Fig. 1) of the reflection coefficient [39,40]. Moreover, at the low energies of interest in STM (usually below the non-specular beam emergence threshold) a one-dimensional LEED model is a good approximation [39–41].

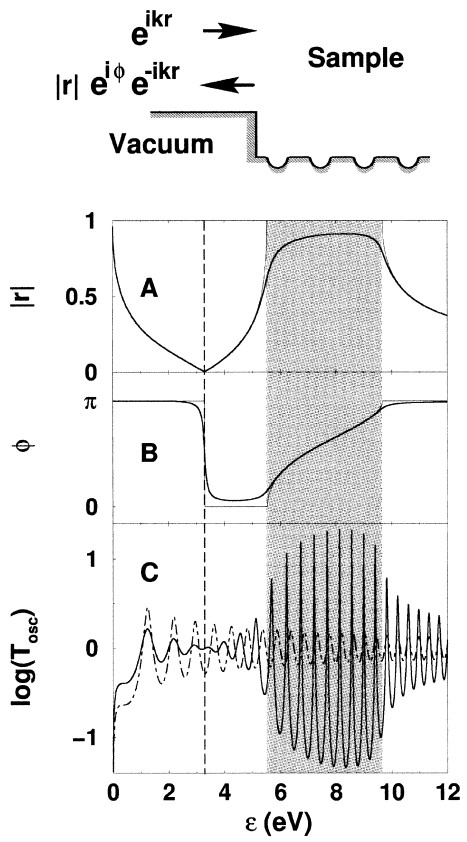

Fig. 2. Calculated modulus $|r|$ (A) and phase ϕ (B) of the reflectance based on the one-dimensional LEED model (sketched on top). Results with (thick lines) and without (thin lines) absorption are shown. (C) Theoretical FER spectrum [$\propto\log(T_{osc})$] with absorption (thick line). Results for a free electron sample (dot-dashed line) are shown for comparison. Disruptions in FER spectra as well as the phase shifts are shown to be clearly associated with details of the reflectance of the sample surface. The shaded zone represents the gap in the band structure of the crystal.

The tip–vacuum–sample potential is modelled by the simple trapezoidal barrier in the inset of Fig. 1. As in the original Gundlach approach [8], the electron wavefunctions in the vacuum are given by a linear combination of Airy functions. Taking into account the reflectance, r, and after appropriate matching of the wave functions, the total transmission probability, T (at the tip Fermi level), takes the simple expression:

$$T(\epsilon)\approx\left[\frac{4\sqrt{E_F W_t}}{E_F+W_t}\exp\left(-a\,\frac{W_t^{3/2}}{F_t}\right)\right]T_{osc}, \qquad (2)$$

$$T_{osc}=\left[\frac{1-|r|^2}{1+|r|^2-2|r|\sin(2\xi-\phi)}\right], \qquad (3)$$

where $a=(4/3)\sqrt{2m}/\hbar$ and $\xi=a\epsilon^{3/2}/F_s$, and the Airy wave functions have been approximated by their asymptotic series. The first term of Eq. (2) is readily recognized as the standard F–N term [32], which is obtained in the absence of any electron coherence. The semiclassical S–V curve corresponds to $T_{F\text{–}N}=$constant. The main effect of the second term is to induce the small quantum oscillations

$$\Delta S\approx\frac{SF_t}{aW_t^{3/2}}\ln(T_{osc}). \qquad (4)$$

$\Delta S(V)$ presents oscillations with a shape and amplitude that generally depend on the working conditions (tip work function, tip radius, total intensity[1], …). The period of the oscillations is a function of the sample phase shift $\phi(\epsilon)$ and field F_s and presents maxima at voltages V_n given by

$$\phi(\epsilon)=\frac{2a}{F_s}(eV_n-W_s)^{3/2}-\left(2n\pi-\frac{\pi}{2}\right), \qquad (5)$$

where n indicates the order of the peak[1]. The important result is that the phase shift obtained from the resonance condition is a property of the sample surface in the absence of a tip and field. Measuring the resonance voltages, V_n, then give us a direct measure of the phase shift $\phi(\epsilon)$ as a function of the energy. The resolution in energies depends on the number of maxima observed within the experimental window of bias voltages (an analogous expression for the minima can be used to double the resolution). For a given tip radius (working intensity), decreasing the working intensity (increasing the tip radius) leads to lower working fields, which increases the number of peaks in a given voltage window [17,18]. Experiments at different intensities and/or with different tip radius could then be used to determine the $\phi(\epsilon)$ curve.

[1] It is usually considered that the current in the field emission regime is determined by the tunneling of the electrons at the Fermi level. As shown by numerical calculations [20–24], integration to all electron energies only diminshes the amplitude of the oscillations but leaves the peaks' positions unchanged.

In order to illustrate the physics contained in the ΔS versus V curves [Eq. (4)], and to understand the experimental phase shifts, let us consider some general properties of the surface reflectance. In Fig. 2A and B, we have plotted the results for the reflection coefficient $|r(\epsilon)|$ and phase shift $\phi(\epsilon)$ based on a simple one-dimensional LEED model[2]. In general, the bulk electronic band gaps manifest themselves as strong peaks in the reflection coefficient. As the energy sweeps across one of these gaps, there is a π shift in the phase of the reflected electrons [29]. At some given energies, r may also vanish as a consequence of a perfect matching of the electron wave functions in the vacuum–sample interface. In this case, there is also a π shift in the phase but with the opposite sign. The fading and reappearance of experimental FER spectra can be associated with this perfect matching condition. This can be clearly seen in Fig. 2C, where we have plotted the calculated (T_{osc}) spectrum (for $F_s \approx 0.2$ V Å^{-1}). Notice that, in contrast with the band-gap shift, the zero reflectance shift is not an intrinsic property of the long-range crystalline order. This suggests a common physical origin of the puzzling disturbances observed in both crystalline and amorphous samples.

From the above theoretical picture, we can obtain and analyse experimental spectra in a simple way. As an example, we will analyse the FER spectra of the Pb/Si(111). It is known that Pb chemisorption on Si(111) surfaces induces different reconstructions, depending on the sample preparation conditions. In particular, at Pb coverages lower than 1 monolayer (ML), annealed samples can present a (1×1) phase and two ($\sqrt{3}\times\sqrt{3}$R30) phases, the first one (or β phase) corresponding to a normal coverage of 1/3 ML, and the latter (also called the 'mosaic' phase) corresponding to 1/6 ML [42,43]. In the present study, Pb/Si(111) surfaces that presented the (1×1) phase and the $\sqrt{3}\times\sqrt{3}$R30 − 1/3 ML phases (R3 in the following) were prepared by Pb deposition on Si(111) 7×7 surfaces at coverages of ≤ 1 ML, followed by annealing at ≈ 450°C for several minutes. The experiments were performed in situ using an ultra-high vacuum STM system [44,45]. STM images were acquired in the constant current mode at several bias voltages ranging from ± 0.1 to ± 2 V. Fig. 3 shows typical STM images on Pb/Si(111) annealed samples, where both (1×1)

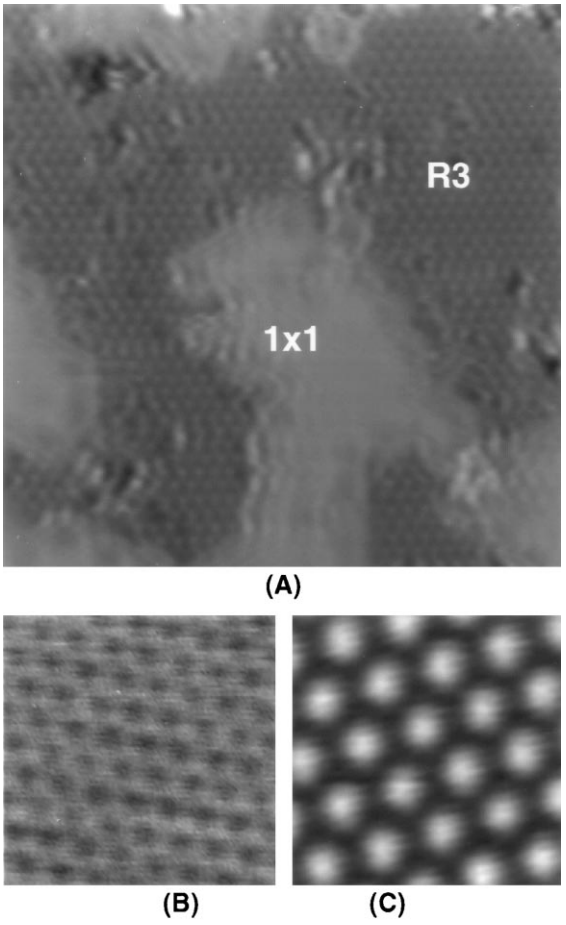

Fig. 3. STM images measured on a Pb/Si(111) annealed sample. (A) Large region (25×25 nm^2) showing the R3 reconstruction, together with several islands showing a 1×1 reconstruction. Tunneling conditions: sample voltage $+2$ V; tunnel current 1 nA. (B) Atomic resolution image of the 1×1 reconstruction. Image size 3×3 nm^2. Tunneling conditions: sample voltage $+0.5$ V; tunnel current 1 nA. (C) Atomic resolution image of the R3 reconstruction Image size 3×3 nm^2. Tunneling conditions: sample voltage $+2.0$ V; tunnel current 1 nA.

[2] We make use of the one-dimensional LEED model described by Pendry in Refs. [39,40]. The calculated reflectance, R, is obtained assuming: $t=0.95$, $V_o=(9-0.2i)$ eV and the lattice constant $c=3$ Å in Pendry's notation. The main qualitative features do not depend on the particular choice of these parameters, however.

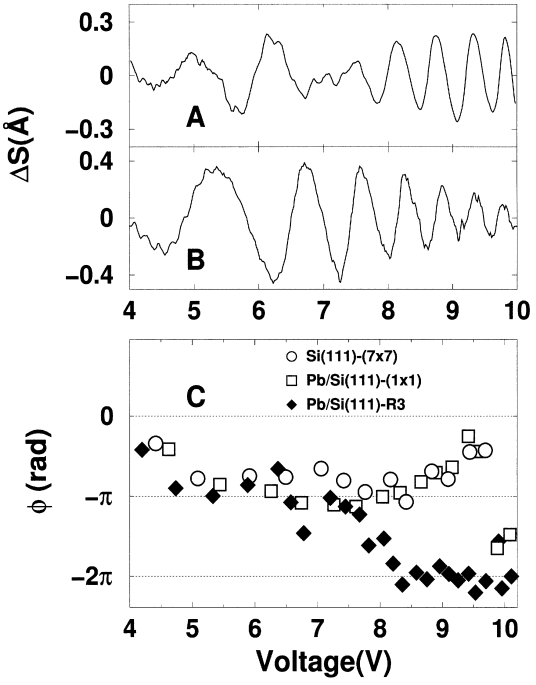

Fig. 4. Experimental FER spectra (ΔS vs. V plots) for the R3 (A) and 1×1 (B) reconstructions. (C) Experimental phase shifts of reflected electron waves for (○) the 7×7 reconstruction of Si(111), (□) the Pb/Si(111)-(1×1) and (◆) the Pb/Si(111)-R3 reconstructions.

and R3 reconstructed regions can be observed. Distance–voltage (S–V) characteristics were measured in different fixed spots on both reconstructions. The vertical displacement, S, of the tip, relative to the original tunnel position, was measured while ramping the bias voltage, V (with the tip at negative polarity) under feedback control.

Fig. 1 shows typical S–V curves measured on R3 regions with two different tips. Except for the small FER-induced oscillations, the observed non-linear behaviour can be understood in terms of the semiclassical $S(V)$ behaviour. The good agreement between experiments and theory [Eq. (1)] is illustrated in Fig. 1. In Fig. 4A and B we show representative experimental ΔS versus V plots for the R3 and (1×1) reconstructions, obtained after substracting the semiclassical component from the experimental S–V curves[3]. As discussed above, a direct measure of $\phi(\epsilon)$ can be obtained from the experimental FER spectra by measuring the voltages, V_n, at which ΔS presents maxima[4]. Fig. 4C shows the energy dependence of the phases for the R3 and (1×1) reconstructions as well as for the clean Si(7×7). Whereas $\phi(\epsilon)$ shows a smooth behaviour for both the clean 7×7 and the (1×1), the R3 structure presents a clear π shift at ≈7 V. Notice that at the same bias, the ΔS spectra present a disturbance [12–19] in the amplitudes of the oscillations. A similar shift at the same voltage was also indirectly deduced by Kubby et al. [17,18] by comparison between the spectra on the 7×7 and on the R3 reconstruction of the Sn/Si(111) taken with the same tip.

Our results demonstrate the ability of the STM to measure the phase of electron waves reflected from the sample surface. On the basis of a simple theory, we have been able to relate the observed features with fundamental properties of the surface. A quantitative explanation of all the features observed requires a more sophisticated study of the scattering processes, including a proper description of the tip–vacuum–sample and the atomic structure of the sample. We envision utilizing the STM images and FER spectra, perhaps in an analogous way to that of LEED structural determination, to probe the atomic and electronic structures of non-periodic surfaces and adsorbates.

Acknowledgements

We thank A. García-Martín, T. López-Ciudad and J.A. Torres for fruitful discussions. This work has been supported by DGICyT through grants No. PB95-0061 and PB95-0169. A.J.C. has been supported by the DGICyT interchange program between industries and public research centres (Grant No. IN92-D00830413) through a joint agreement between RYMSA (Radiación y Microondas, S.A.) and the U.A.M.

[3] In contrast with the standard differential conductance measurements, this method does not need a lock-in amplifier.

[4] The sample work function, W_s, entering Eq. (5) is experimentally determined from the threshold bias for the field emission regime. This gives effective values of ≈4 and ≈4.2 eV for the R3 and 1×1 reconstructions, respectively.

References

[1] A.J. Jason, R.P. Burns, M.G. Inghram, J. Chem. Phys. 43 (1965) 3762.
[2] A.J. Jason, Phys. Rev. 156 (1966) 266.
[3] M.E. Alferieff, C.B. Duke, J. Chem. Phys. 46 (1967) 938.
[4] G.R. Hanson, M.G. Inghram, Surf. Sci. 55 (1970) 29.
[5] E.W. Müller, S.V. Krishnaswamy, Surf. Sci. 36 (1973) 29.
[6] J.A. Appelbaum, E.G. Mcrae, Surf. Sci. 47 (1975) 445.
[7] T.T. Tsong, Atom-probe Field Ion Microscopy, Cambridge University Press, Cambridge, 1990. Sec. 2.1.5.
[8] K.H. Gundlach, Solid State Electron. 9 (1966) 949.
[9] J. Maserjian, J. Vac. Sci. Technol. 11 (1974) 996.
[10] J. Maserjian, N. Zamani, J. Appl. Phys. 53 (1982) 559.
[11] T.W. Hickmott et al., Appl. Phys. Lett. 44 (1984) 90.
[12] G. Binnig, H. Rohrer, Helv. Phys. Acta 55 (1982) 726.
[13] G. Binnig et al., Phys. Rev. Lett. 55 (1985) 991.
[14] R.S. Becker, J.A. Golovchenko, B.S. Swartzentruber, Phys. Rev. Lett. 55 (1985) 987.
[15] R.S. Becker et al., Phys. Rev. Lett. 55 (1985) 2032.
[16] J.H. Coombs, J.K. Gimzewski, J. Microsc. 152 (1988) 841.
[17] J.A. Kubby, Y.R. Wang, W.J. Greene, Phys. Rev. Lett. 65 (1990) 2165.
[18] J.A. Kubby, W.J. Greene, Phys. Rev. B 48 (1993) 11249.
[19] L. Scandella, H.-J. Güntherodt, Ultramicroscopy 42–44 (1991) 546.
[20] R. García et al., J. Phys. C: Solid State Phys. 19 (1986) L131.
[21] R. García et al., Surf. Sci. 181 (1986) 69.
[22] J. Bono, R.H. Good, Surf. Sci. 188 (1987) 153.
[23] J.M. Pitarke, F. Flores, P.M. Echenique, Surf. Sci. 234 (1990) 1.
[24] R. García-García, J.J. Sáenz, Surf. Sci. 251–252 (1991) 223.
[25] M. Grishin et al., Chem. Phys. Rep. 16 (1997) 955.
[26] R. Dashen, S.-K. Ma, H.J. Bernstein, Phys. Rev. B 187 (1969) 345.
[27] Y. Avishai, A. Band, Phys. Rev. B 32 (1985) 2674.
[28] F. García-Moliner, F. Flores, Introduction to the Theory of Solid Surfaces, Cambridge University Press, Cambridge, 1979.
[29] J.B. Pendry, S.J. Gurman, Surf. Sci. 49 (1972) 87.
[30] P.M. Echenique, J.B. Pendry, J. Phys. C: Solid State Phys. 32 (1978) 111.
[31] P.M. Echenique, J.B. Pendry, Prog. Surf. Sci. 32 (1990) 111.
[32] R. Gomer, Field Emission and Field Ionization, Harvard University Press, Cambridge, MA, 1961.
[33] R. Young, J. Ward, F. Scire, Rev. Sci. Instrum. 43 (1972) 999.
[34] J.J. Sáenz, R. García, Appl. Phys. Lett. 65 (1994) 3022.
[35] G. Mesa, J.J. Sáenz, R. García, J. Vac. Sci. Technol. B 14 (1996) 2403.
[36] D.P. Adams, T.M. Mayer, B.S. Swartzentruber, J. Vac. Sci. Technol. B 14 (1996) 1642.
[37] G. Mesa, E. Dobado-Fuentes, J.J. Sáenz, J. Appl. Phys. 79 (1996) 39.
[38] G. Mesa, E. Sáenz, Appl. Phys. Lett. 69 (1996) 1169.
[39] J.B. Pendry, Low Energy Electron Diffraction, Academic Press, London, 1974.
[40] M.A. van Hove, S.Y. Tong, Surface Crystallography by LEED, Springer, Berlin, 1979.
[41] H. Iwasaki, B.T. Jonker, R.L. Park, Phys. Rev. B 32 (1985) 643.
[42] E. Ganz et al., Phys. Rev. B 43 (1991) 7316.
[43] E. Ganz et al., Surf. Sci. 257 (1991) 259.
[44] J.M. Gómez-Rodriguez et al., Phys. Rev. Lett. 76 (1996) 799.
[45] J.M. Gómez-Rodriguez et al., Surf. Sci. 377–379 (1997) 45.